Electronic Supplementary Material (ESI) for Journal of Materials Chemistry A.

Electronic Supplementary Information

Mixed Phthalocyanine-Porphyrin-Based Conjugated Microporous Polymers towards Unveiling the Activity Origin of Fe-N_4 Catalysts for Oxygen Reduction Reaction

Wenbo Liu,[‡a] Kang Wang,[‡a] Chiming Wang,[a] Wenping Liu,[a] Houhe Pan,[a] Yanjuan Xiang,[b] Dongdong Qi,*[a] and Jianzhuang Jiang*[a]

Experimental Section

Characterization. The ^{13}C CP/MAS NMR spectra were recorded with a 4-mm MAS probe and with a sample spinning rate of 3.0 kHz. IR spectra were recorded as KBr pellets using a Bruker Tensor 37 spectrometer with 2 cm^{-1} resolution. Powder X-ray diffraction (PXRD) data were collected on a Shimadzu XRD-6000 diffractometer using Cu-Kα radiation (I = 1.54056 Å) at room temperature. SEM images were obtained using a JEOL JEM-6510A scanning electron microscopy. Transmission electron microscopy (TEM) was measured by HT7700 electron microscope at 100 KV. HR-TEM was measured by JEOL 2200FS electron microscope at 200 KV. HAADF-STEM images and energy dispersive spectros-copy (EDS) mapping images were taken on a JEM-ARM200F electron microscope operated at 200 kV. The Fe and Zn contents of the M_1PcM_2Por-CMPs were determined by inductively coupled plasma atomic emission spectroscopy (ICP-AES) analysis with an IRIS Intrepid II XRP instrument. XPS measurements were carried out on PHI 5300 ESCA System (PerkineElmer, USA). Solid-state UV-Vis diffuse reflectance spectra were recorded on an SHIMADZU UV-2600 spectrophotometer. TGA measurements were performed on a PerkinElmer TG-7 analyzer with a heating rate of 10 °C min^{-1} in the range of 25-900 °C under N_2 atmosphere.

Electrochemical tests. Electrochemical measurements were all conducted on the CHI 760E workstation (CH Instruments, Inc.) with a RRDE-3A rotator (ALS Co., Ltd). The typical three-electrode system was employed to evaluate the electrochemical properties of the as-prepared catalysts. Specifically, glassy carbon was the working electrode, a Pt wire was the counter electrode, and the Ag/AgCl (in saturated KCl solution) was the reference electrode. All potentials were referred to the reversible hydrogen electrode by adding a value of

(0.197+0.059×pH) V. The catalyst ink was prepared by dispersing 4 mg of sample [50% M_1PcM_2Por-CMPs and 50% carbon black (Vulcan XC-72)] into 1 mL ethanol solvent containing 20 μL 5wt% Nafion and sonicated for 60 min. Then, 5 μL of the mixture was dropped onto a polished glassy carbon electrode (4 mm in diameter). The loaded electrode was placed in a 60 °C oven for 30 min to dry and then was taken out to cool down before all the tests. The corresponding catalyst loading is 0.16 mg cm^{-2}. Cyclic voltammetry (CV) experiments were recorded at the scan rate of 50 mV s^{-1} under static conditions in O_2-saturated and O_2-free 0.1 M KOH solution. The RDE polarization curves were recorded under various rotation rates at the scan rate of 10 mV s^{-1} in O_2-saturated 0.1 M KOH solution. For the methanol tolerance test, after injecting 5 % (volume) methanol into the cell, the electrode was rotated for 5 min to ensure the added methanol dispersed homogeneously in the O_2-saturated electrolyte, and then the CV measurement was carried out under static conditions again. The durability of catalysts was evaluated by performing the chronoamperometric measurement in the O_2-saturated solution for 20000 s. All the electrochemical tests in this study were conducted at least three times to ensure the accuracy of the measurement. Besides, the iR correction was applied to get rid of the influence of the Ohmic resistance, and the effect of the doublelayer capacitance on the ORR performance of the resulting catalysts was eliminated.

Rotating ring-disk electrode (RRDE) measurement. The rotating speed of the working electrode was fixed at 1600 rpm with the scan rate of 10 mV s^{-1} for the RRDE test. The electron transfer number (n) is calculated via the following equation.[S1]

$$n = 4I_d / (I_d + I_r / N)$$

$$\% HO^{2-} = 200(I_r / N) / (I_d + I_r / N)$$

Where I_d stands for the disk current, I_r represents the ring current, and N is the current collection efficiency of the Pt ring, which was identified to be 0.43 in 2 mmol L^{-1} $K_3Fe[CN]_6$ and 0.1 M KCl solution.

Koutecky-Levich (K-L) plots. The working electrode was scanned cathodically at the rate of 10 mV s^{-1} with the rotation speed from 400 to 2500 rpm. Koutecky-Levich (K-L) plots (J^{-1} *vs* $\omega^{-1/2}$) were analyzed at 0.3-0.7 V. Koutecky-Levich equation:[S2,S3]

$$1/J = 1/J_L + 1/J_K = 1/(B\omega^{1/2}) + 1/J_K$$

$$B = 0.2nFC_0D_0^{2/3}v^{-1/6};\ J_K = nFkC_0$$

Where J is the measured current density, J_K and J_L are the kinetic and limiting current densities, ω is the angular velocity, n is transferred electron number, F (96485 C mol^{-1}) is the Faraday constant, D_0 is the diffusion coefficient of O_2 in 0.1 M KOH (1.9×10^{-5} cm^2 s^{-1}), C_0 is the bulk concentration of O_2 (1.2×10^{-6} mol cm^{-3}), v is the kinetic viscosity of the electrolyte (0.01 cm^2 s^{-1}), and k is the electron-transfer rate constant. The constant 0.2 is adopted when the rotation speed is expressed in rpm.

Mass Activity. The mass activity was obtained by normalizing the kinetic current (I_k) to the electrode mass. I_k is obtained by multiplying J_k (derived from the Koutecky-Levich equation at 0.9 V vs RHE) with the geometric area of the glassy carbon disk.

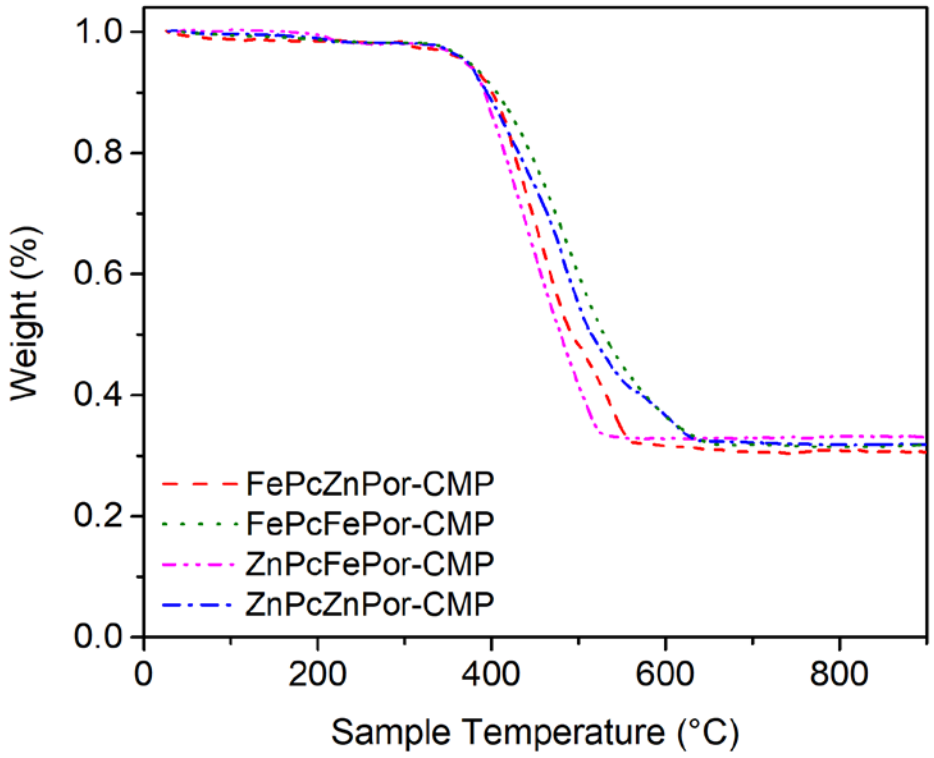

Fig. S1 TGA of FePcZnPor-CMP, ZnPcFePor-CMP, FePcFePor-CMP, and ZnPcZnPor-CMP.

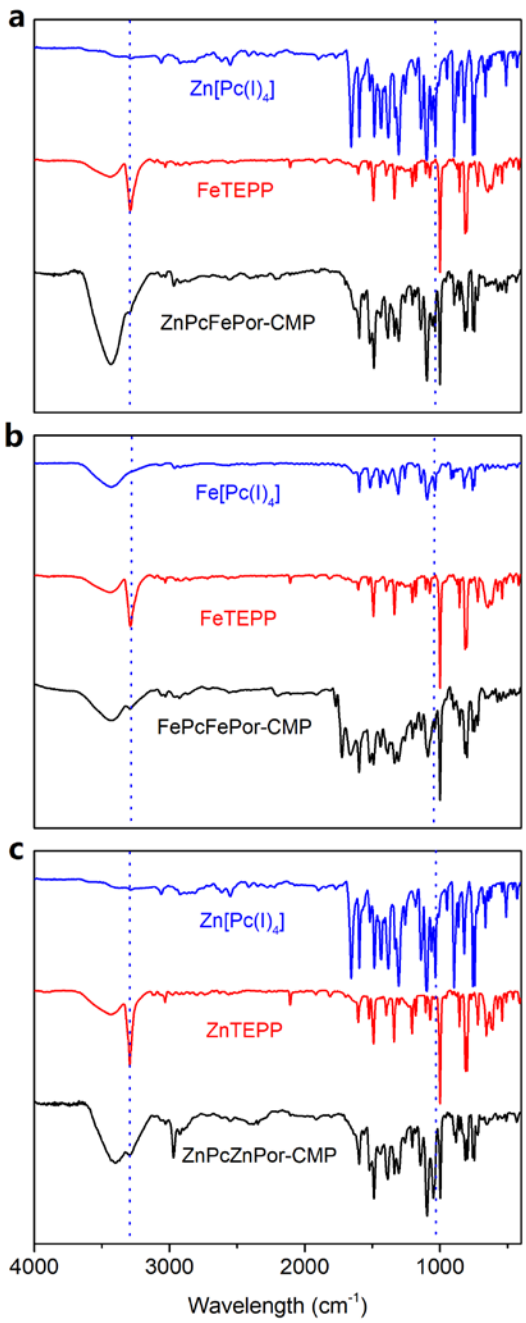

Fig. S2 FT-IR spectra of (a) ZnPcFePor-CMP, (b) FePcFePor-CMP, and (c) ZnPcZnPor-CMP as well as the corresponding phthalocyanine and porphyrin monomers in the region of 400-4000 cm^{-1}.

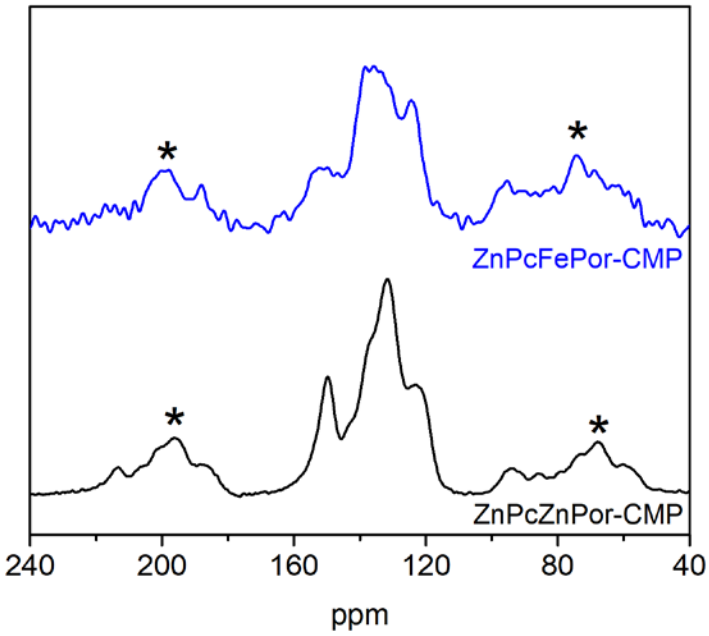

Fig. S3 ^{13}C CP/MAS NMR spectra of ZnPcFePor-CMP and ZnPcZnPor-CMP. Signals with * are sidebands.

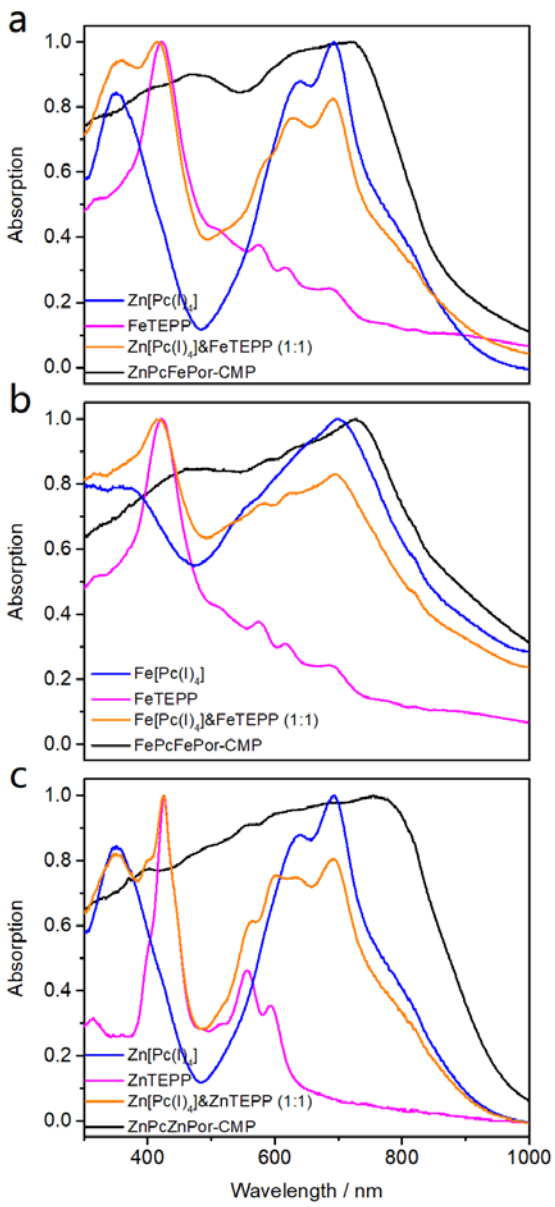

Fig. S4 UV-vis diffuse reflectance spectra of (a) ZnPcFePor-CMP, (b) FePcFePor-CMP, and (c) ZnPcZnPor-CMP as well as the corresponding phthalocyanine and porphyrin monomers.

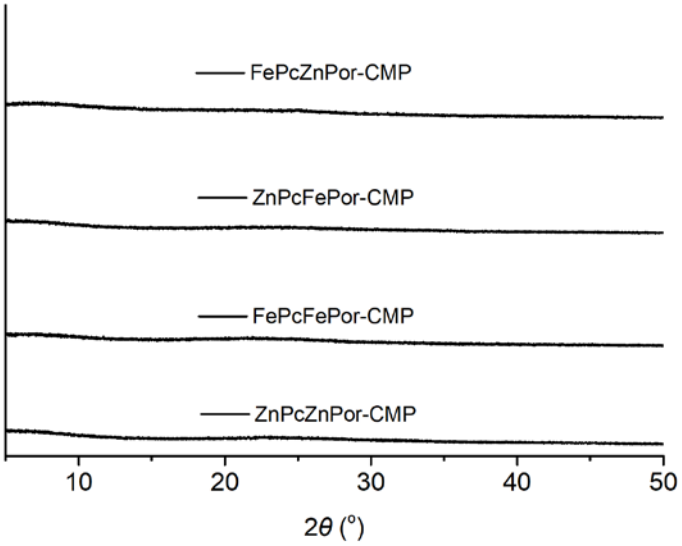

Fig. S5 PXRD patterns of FePcZnPor-CMP, ZnPcFePor-CMP, FePcFePor-CMP, and ZnPcZnPor-CMP.

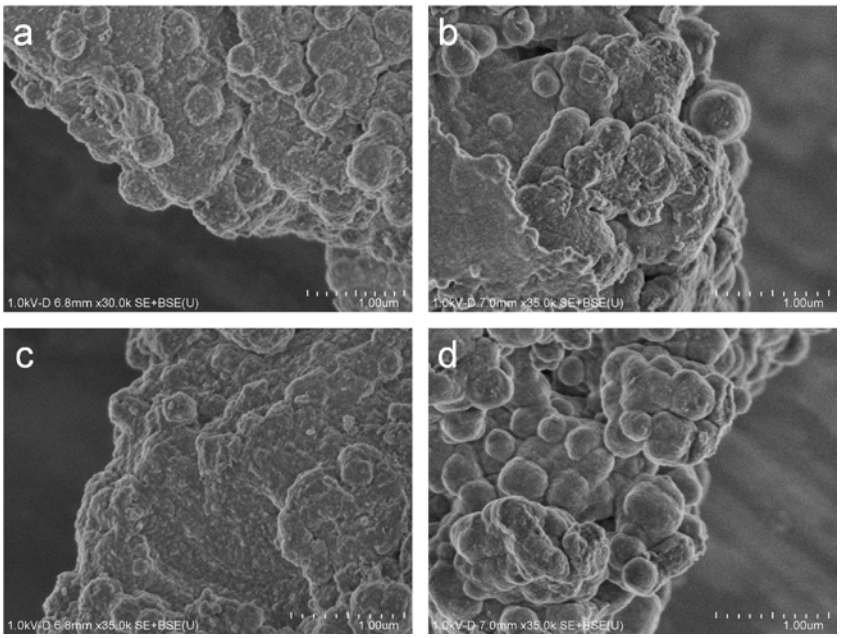

Fig. S6 SEM images of (a) FePcZnPor-CMP, (b) ZnPcFePor-CMP, (c) FePcFePor-CMP, and (d) ZnPcZnPor-CMP.

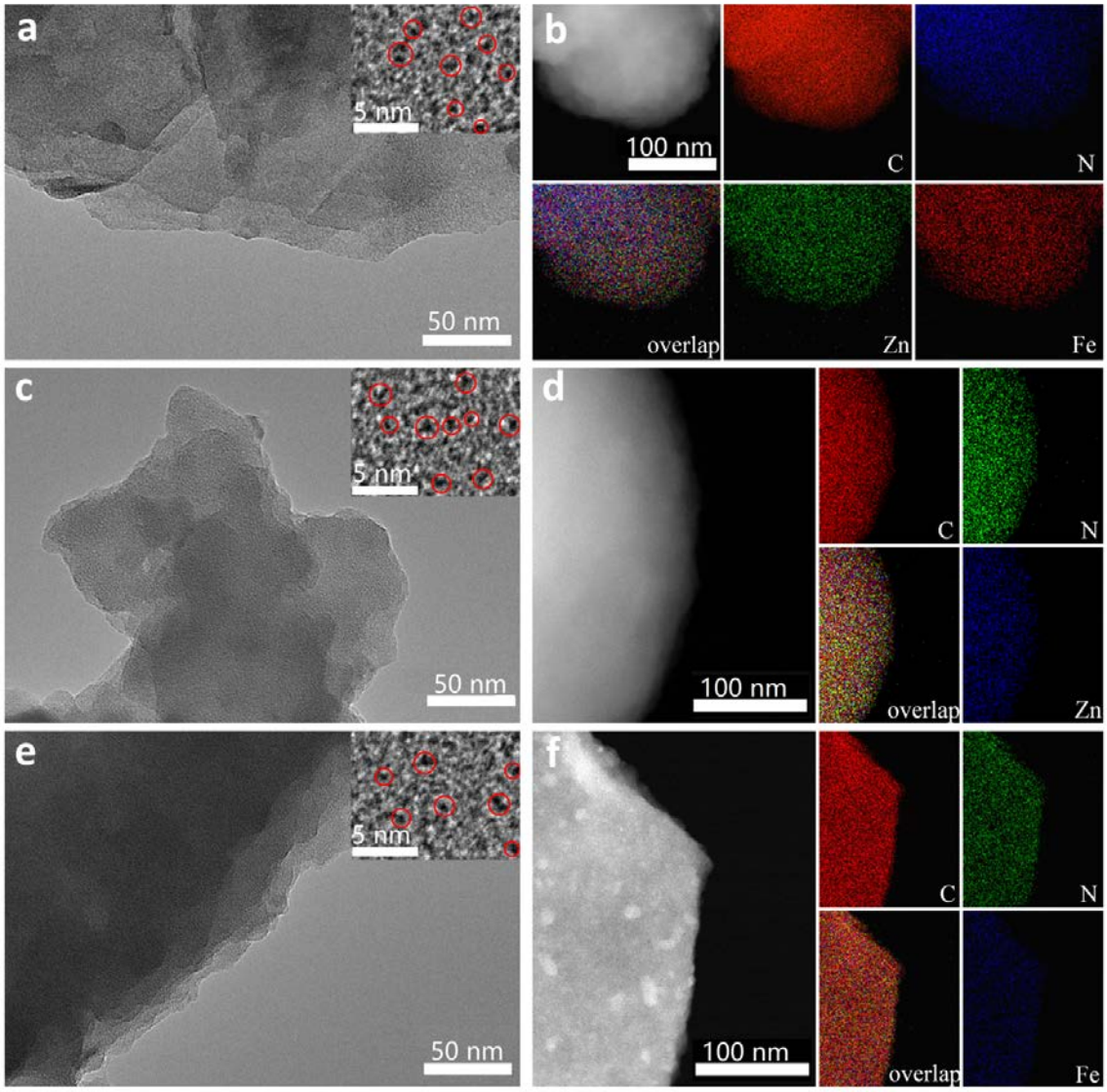

Fig. S7 HR-TEM images of (a) ZnPcFePor-CMP, (c) FePcFePor-CMP, and (e) ZnPcZnPor-CMP. Inset: magnified image of ZnPcFePor-CMP, FePcFePor-CMP, and ZnPcZnPor-CMP. Nanometer-scale cavities highlighted by red circles. The STEM and elemental-mapping images of (b) ZnPcFePor-CMP, (d) FePcFePor-CMP, and (f) ZnPcZnPor-CMP.

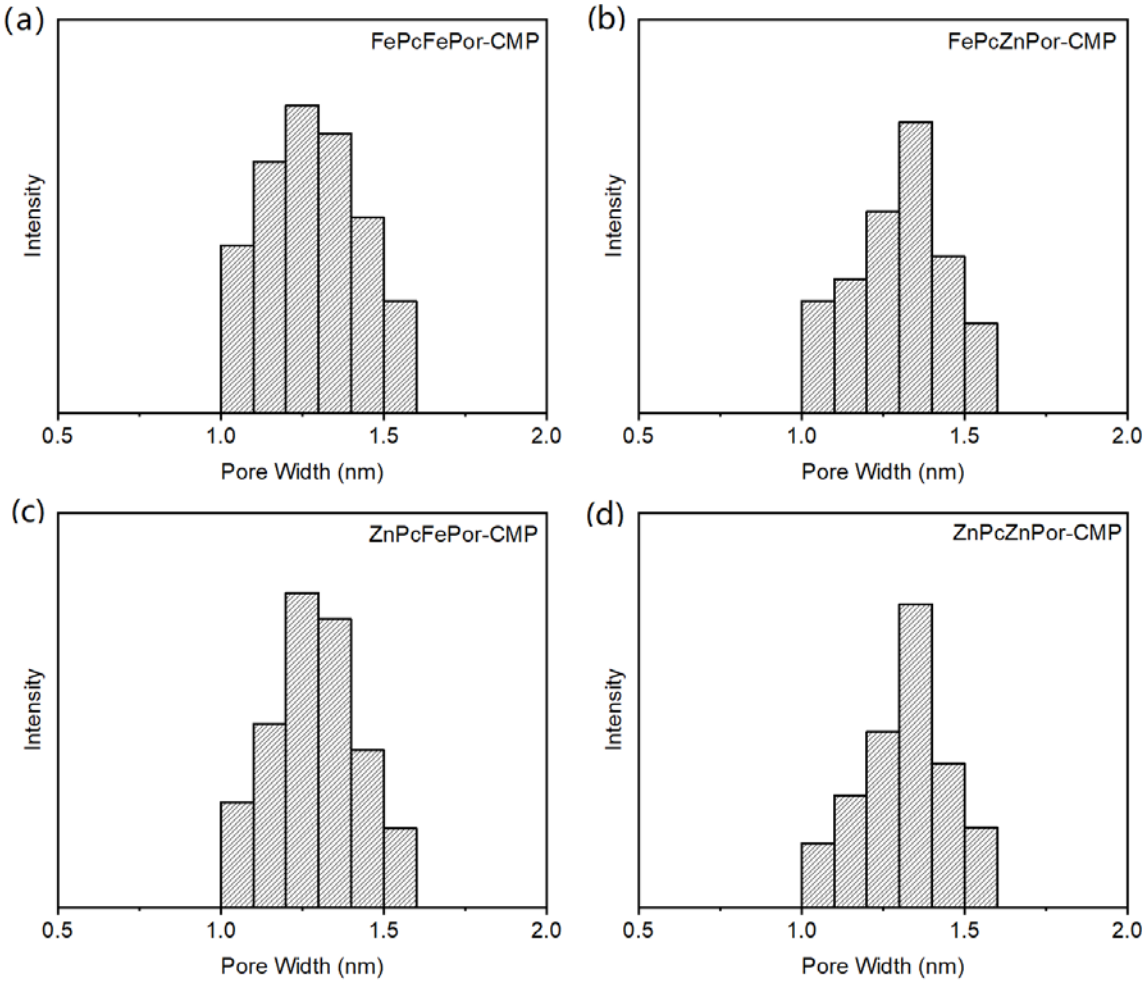

Fig. S8 The pore size distribution of nanometer-scale cavities observed in the HR-TEM images of (a) FePcFePor-CMP, (b) FePcZnPor-CMP, (c) ZnPcFePor-CMP, and (d) ZnPcZnPor-CMP.

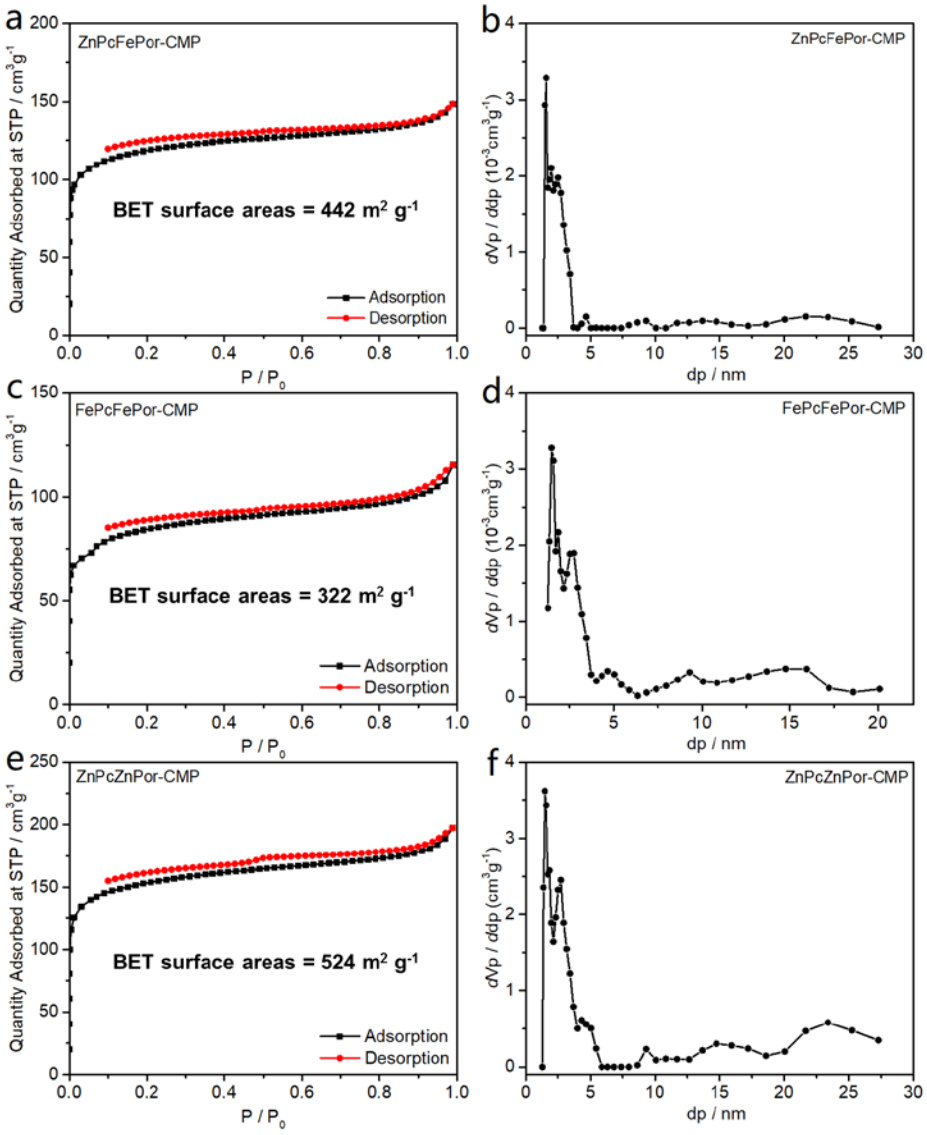

Fig. S9 N_2 adsorption−desorption isotherms (77 K) and pore size distribution of (a, b) ZnPcFePor-CMP, (c, d) FePcFePor-CMP, and (e, f) ZnPcZnPor-CMP

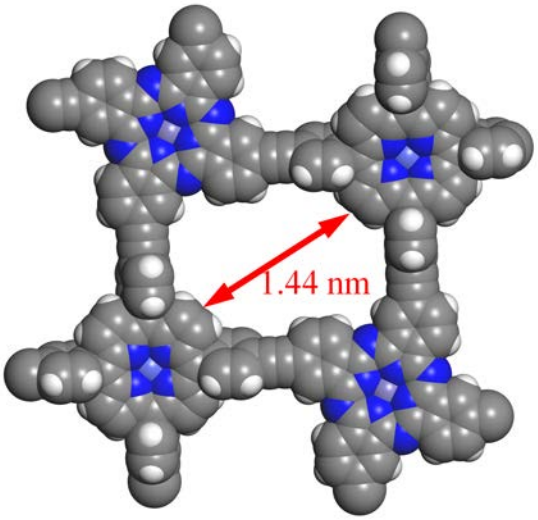

Fig. S10 Optimized structure of $(FePcZnPor)_2$ moiety as the representative minimum unit for M_1PcM_2Por-CMPs, which show the pore width of *ca*. 1.44 nm..

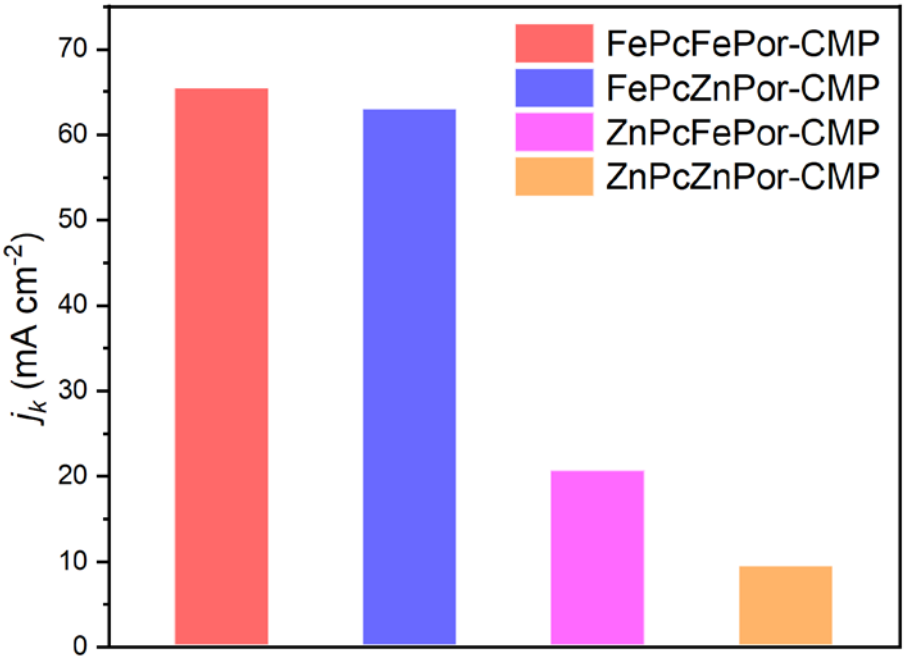

Fig. S11 The comparison of the kinetic current density at 0.5 V vs RHE demonstrated in O_2-saturated 0.1M KOH solution on M_1PcM_2Por-CMP-loaded glassy carbon electrodes.

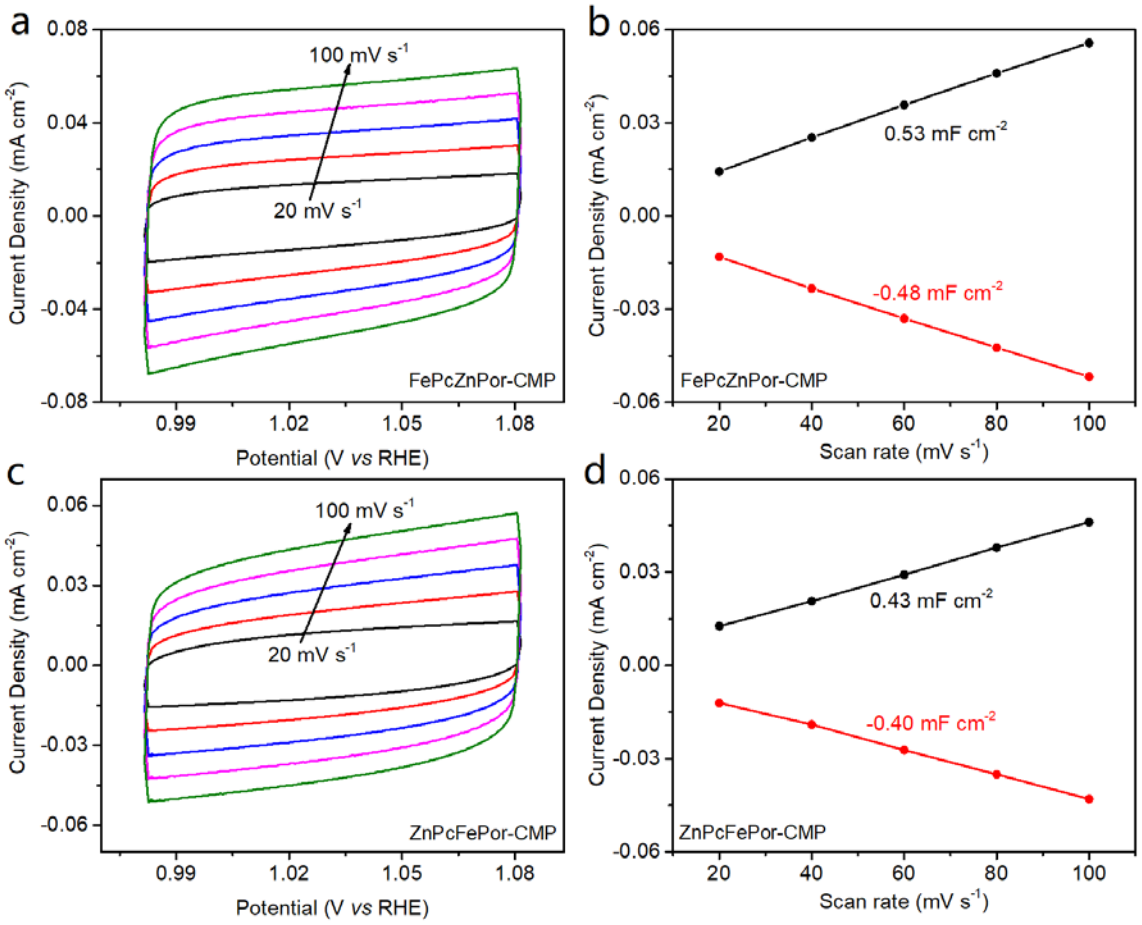

Fig. S12 (a)(c) CV conducted at potential from 0.98 V to 1.08 V *vs* RHE at scan rates of 20 mV s^{-1}, 40 mV s^{-1}, 60 mV s^{-1}, 80 mV s^{-1}, and 100 mV s^{-1} in 0.1 M KOH. (b)(d) The current densities of anode and cathode measured at 1.03 V *vs* RHE with different scan rates. (a)(b) and (c)(d) are FePcZnPor-CMP with 50 wt% XC-72 and ZnPcFePor-CMP with 50 wt% XC-72, respectively.

To study the electrochemically active surface areas (ECSAs) of FePcZnPor-CMP with 50 wt% XC-72 and ZnPcFePor-CMP with 50 wt% XC-72, we conducted the CV cycles at different scan rates during the potential from 0.98 V to 1.08 V vs RHE in 0.1 M KOH, where there is no Faradic current. At last, the ECSA was estimated from the as obtained double-layer capacitance (Cdl). According to Cdl is constant, it can be calculated as:

$$Cdl = Q/U = (dQ/dt)/(dU/dt) = j/r \quad (1)$$

Q is the quantity of electric charge per unit area,

U is the voltage,

j is the current density

r is the scan rate.

From Eq(1), the Cdl is the slope of j~r, which can be obtained by the Figure S12b and S12d. The average Cdl of FePcZnPor-CMP with 50 wt% XC-72 and ZnPcFePor-CMP with 50 wt% XC-72 are 0.51 mF/cm^2 and 0.42 mF/cm^2, respectively. The ECSA can be calculated as:

$$ECSA = Cdl/Cs \quad (2)$$

Cs is the specific capacitance value for a flat standard with 1 cm^2 of real surface area. The general value for Cs is between 20 μF/cm^2 and 60 μF/cm^2. Here we use 40 μF/cm^2 as the average value (Nat. Commun. 2015, 6, 8668). Thus the ECSA for FePcZnPor-CMP with 50 wt% XC-72 and ZnPcFePor-CMP with 50 wt% XC-72 can be obtained as 13 cm^2 and 11 cm^2, respectively.

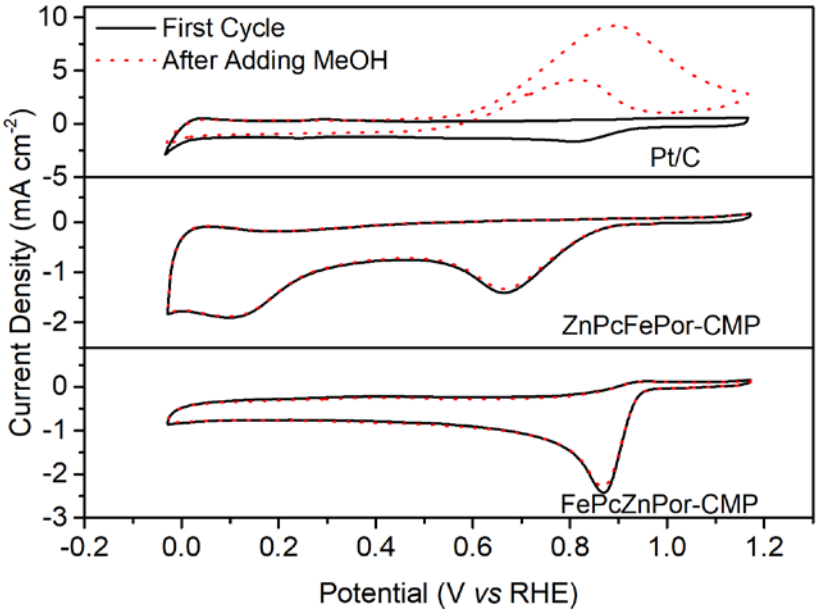

Fig. S13 Methanol tolerance test with 5% methanol (in volume) in O_2-saturated 0.1 M KOH solution for FePcZnPor-CMP, ZnPcFePor-CMP, and Pt/C (20%) (the CV scan rate is 50 mV s^{-1}).

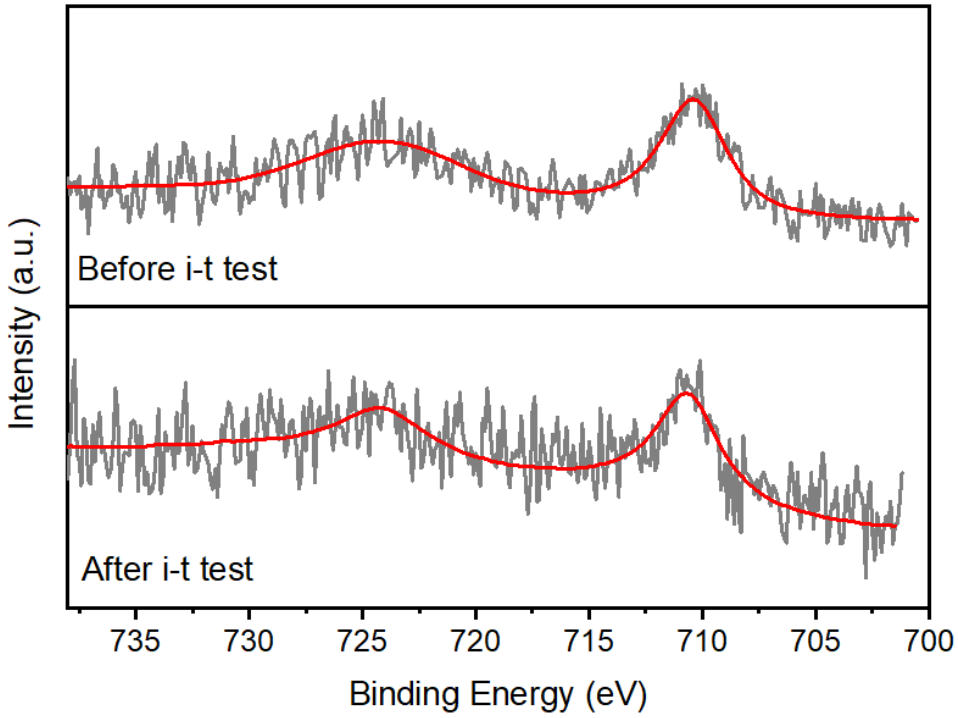

Fig. S14 XPS high resolution Fe 2p spectra of FePcZnPor-CMP before and after i-t test. Almost the same XPS high resolution Fe 2p spectra of FePcZnPor-CMP before and after i-t test confirm the high stability of FePcZnPor-CMP.

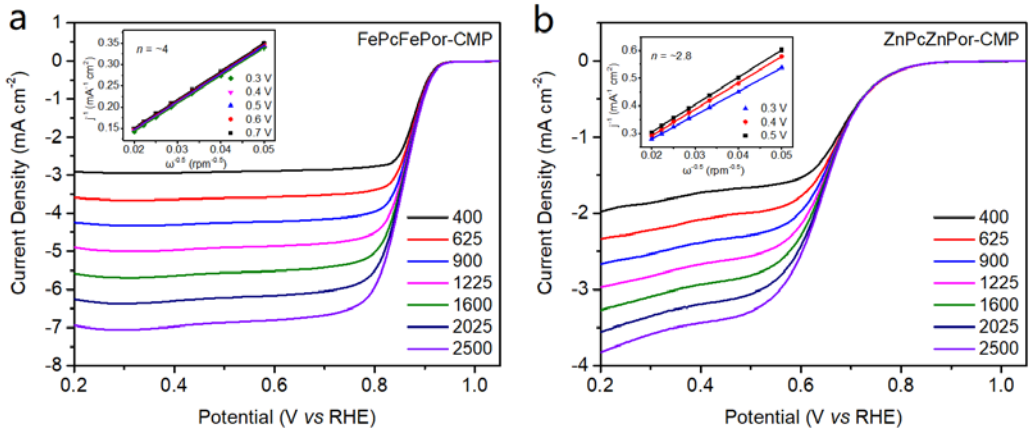

Fig. S15 LSV curves of (a) FePcFePor-CMP and (b) ZnPcZnPor-CMP at different rotation speeds. Insert: Koutecky–Levich (K–L) plots at different potentials.

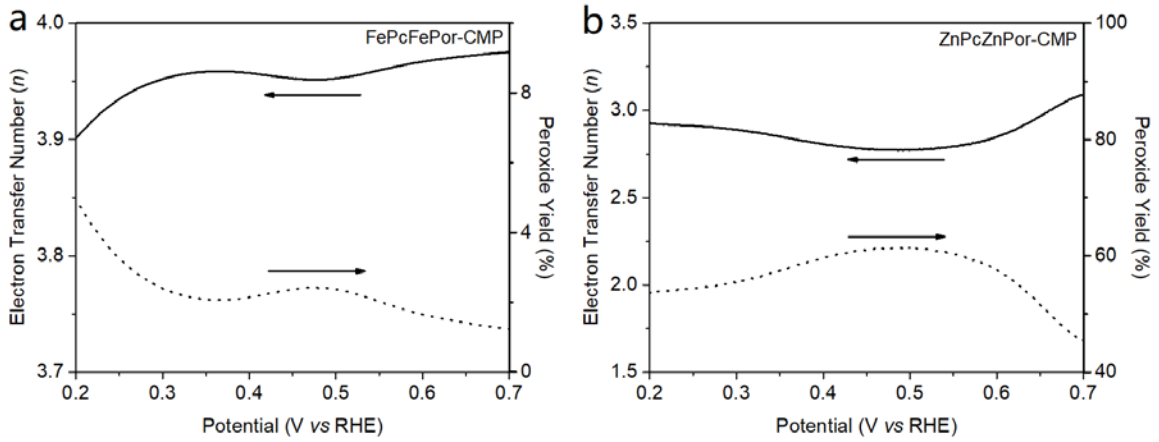

Fig. S16 Percentage of peroxide species (dotted solid lines) and the electron-transfer number (*n*) (solid lines) of (a) FePcFePor-CMP and (b) ZnPcZnPor-CMP in the potential range of 0.20-0.70 V (calculated from the corresponding RRDE data).

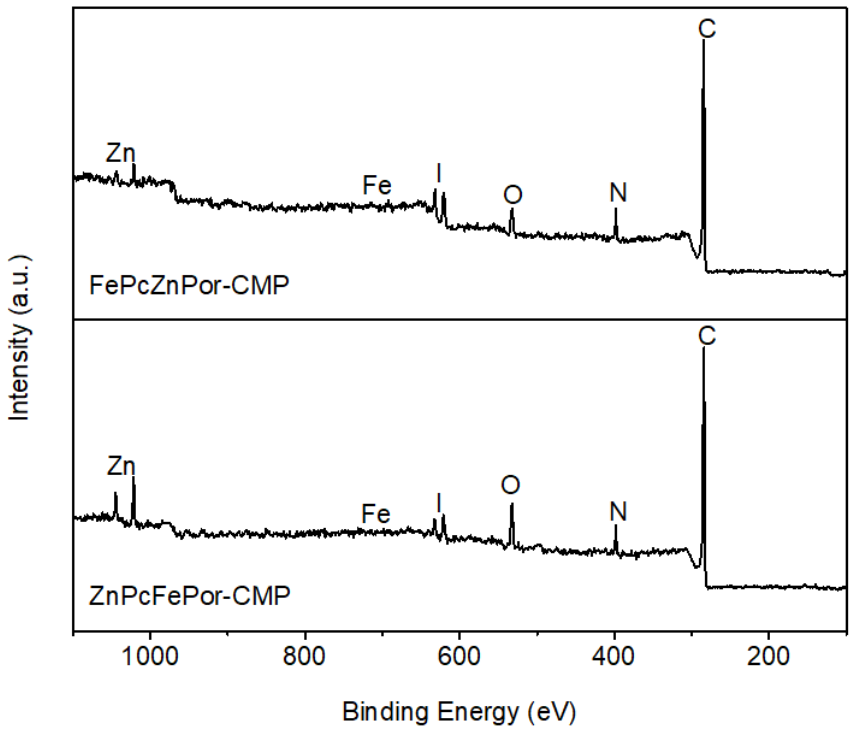

Fig. S17 XPS overall spectra of FePcZnPor-CMP and ZnPcFePor-CMP.

Table S1. The electrochemical properties for the selected Fe-N_4 based ORR catalysts reported thus far and this work in alkaline media.

Catalyst	E_{onset} [V *vs* RHE]	$E_{1/2}$ [V *vs* RHE]	$\|J_L\|$ [mA cm^{-2}]	Ref
ZnPcFePor-CMP	0.902	0.724	-5.31	This work
FePcFePor-CMP	0.934	0.863	-5.57	This work
FePcZnPor-CMP	0.936	0.866	-5.59	This work
$(FeP)_n$-CNTs	0.88	0.76	-4.7	S4
FePPc/CNT-1.5	/	0.93	-5.8	S5
CNT-PC	0.95	0.88	-6.0	S6
FePhenMOF-$ArNH_3$	0.98	0.78	-6.3	S7
HNCS71	0.97	0.82	-6.5	S8
BP_{OX}-NFe	1.07	0.9	-6.2	S9
FePc/KJ300	/	0.62	-3.8	S10
Fe-N-C	1.08	0.88	-5.5	S11
Fe-N-C-950	0.92	0.78	-5.9	S12
FeSAs/PTF-600	1.01	0.87	-5.51	S13
Fe-N-C-AH	0.942	0.848	-6.7	S14
Fe-N_4 SAs/NPC	0.972	0.885	-5.5	S15
Fe-N-HPC-AH	0.97	0.87	-5.4	S16
Fe2-Z8-C	0.902	0.805	-5.5	S17
FePhenMOF-$ArNH_3$	1.05	0.87	-6.1	S18

References

[S1] Y. Liang, Y. Li, H. Wang, J. Zhou, J. Wang, T. Regier and H. Dai, *Nat. Mater.*, 2011, **10**, 780-786.

[S2] Y. Liang, H. Wang, J. Zhou, Y. Li, J. Wang, T. Regier and H. Dai, *J. Am. Chem. Soc.*, 2012, **134**, 3517-3523.

[S3] (a) S. Wang, D. Yu, L. Dai, D. W. Chang and J.-B. Baek, *ACS Nano*, 2011, **5**, 6202-6209; (b) H. T. Bui, N. K. Shrestha, K. Cho, C. Bathula, H. Opoku, Y.-Y. Noh and S.-H. Han, *J. Electroanal. Chem.*, 2018, **828**, 80-85.

[S4] H. Jia, Z. Sun, D. Jiang, S. Yang and P. Du, *Inorg. Chem. Front.*, 2016, **3**, 821-827.

[S5] X. Wang, B. Wang, J. Zhong, F. Zhao, N. Han, W. Huang, M. Zeng, J. Fan and Y. Li, *Nano Res.*, 2016, **9**, 1497-1506.

[S6] Y. J. Sa, D. J. Seo, J. Woo, J. T. Lim, J. Y. Cheon, S. Y. Yang, J. M. Lee, D. Kang, T. J. Shin, H. S. Shin, H. Y. Jeong, C. S. Kim, M. G. Kim, T. Y. Kim and S. H. Joo, *J. Am. Chem. Soc.*, 2016, **138**, 15046-15056.

[S7] J. Li, S. Ghoshal, W. Liang, M.-T. Sougrati, F. Jaouen, B. Halevi, S. McKinney, G. McCool, C. Ma, X. Yuan, Z.-F. Ma, S. Mukerjee and Q. Jia, *Energ. Environ. Sci.*, 2016, **9**, 2418-2432.

[S8] J. Sanetuntikul, C. Chuaicham, Y.-W. Choi and S. Shanmugam, *J. Mater. Chem. A*, 2015, **3**, 15473-15481.

[S9] P. Song, Y. Zhang, J. Pan, L. Zhuang and W. Xu, *Chem. Commun.*, 2015, **51**, 1972-1975.

[S10] M. H. Seo, D. Higgins, G. Jiang, S. M. Choi, B. Han and Z. Chen, *J. Mater. Chem. A*, 2014, **2**, 19707-19716.

[S11] L. Gu, L. Jiang, X. Li, J. Jin, J. Wang and G. Sun, *Chinese J. Catal.*, 2016, **37**, 539-548.

[S12] M. Xiao, J. Zhu, L. Ma, Z. Jin, J. Ge, X. Deng, Y. Hou, Q. He, J. Li, Q. Jia, S. Mukerjee, R. Yang, Z. Jiang, D. Su, C. Liu and W. Xing, *ACS Catal.*, 2018, **8**, 2824-2832.

[S13] J.-D. Yi, R. Xu, Q. Wu, T. Zhang, K.-T. Zang, J. Luo, Y.-L. Liang, Y.-B. Huang and R. Cao, *ACS Energy Lett.*, 2018, **3**, 883-889.

[S14] Z. Qian, Z. Hu, Z. Zhang, Z. Li, M. Dou and F. Wang, *Catal. Sci. Technol.*, 2017, **7**, 4017-4023.

[S15] Y. Pan, S. Liu, K. Sun, X. Chen, B. Wang, K. Wu, X. Cao, W. C. Cheong, R. Shen, A. Han, Z. Chen, L. Zheng, J. Luo, Y. Lin, Y. Liu, D. Wang, Q. Peng, Q. Zhang, C. Chen and Y. Li, *Angew. Chem. Int. Ed.*, 2018, **57**, 1-6.

[S16] H. Li, Z. Zhang, M. Dou and F. Wang, *Chem. Eur. J.*, 2018, **24**, 1-10.

[S17] Q. Liu, X. Liu, L. Zheng and J. Shui, *Angew. Chem. Int. Ed.*, 2018, **57**, 1204-1208.

[S18] J. Li, Q. Jia, S. Ghoshal, W. Liang and S. Mukerjee, *Langmuir*, 2017, **33**, 9246-9253.